SAND2015-6239J

Low Adiabat Compression of Liquid Deuterium Filled Cylindrical Liners to 0.1–2 Gbar

P. F. Knapp, M. R. Martin, D. Dalton, D. H. Dolan, J.-P. Davis, D. H. Romero,
K. Cochrane, G. Loisel, T. R. Mattsson, R. D. McBride, D. B. Sinars
Sandia National Laboratories, Albuquerque, New Mexico, 87185
(Dated: July 15, 2015)

We report on experiments where cylindrical beryllium liners filled with liquid deuterium were compressed to extreme pressure and density with current pulse shaping. In one set of experiments the pressure at stagnation is inferred to be $\gtrsim$ 100 Mbar using penetrating radiography. A peak liner convergence ratio (initial radius over final radius) of 7.6 was measured resulting in an average deuterium density of 10 g/cm^3 and areal density of 0.45 g/cm^2. The stagnation shock propagating radially outward through the liner wall was directly measured with a strength of $\approx$ 120 Mbar. In a second set of experiments the liner was imploded to a peak convergence of 19 resulting in a density of 55 g/cm^3 and areal density of 0.5 g/cm^2. The pressure at stagnation in this experiment is estimated to be $\sim$ 2 Gbar. This platform enables the study of high-pressure, high-density, implosion deceleration and stagnation dynamics at spatial scales that are readily diagnosable ($R \sim 0.1 - 0.4$ mm). Thus, these experiments are directly relevant to both Inertial Confinement Fusion and the study of material properties under extreme conditions.

The creation and diagnosis of extremely dense objects at high pressure in the laboratory is of central importance to the studies of gas giant planets[1–3], astrophysics[3–5] and inertial confinement fusion (ICF)[6–8]. In this Letter we demonstrate the experimental diagnosis of cold ($T \sim 5 - 30$ eV), high pressure ($P \sim 0.1 - 2$ Gbar) deuterium samples using magnetically driven cylindrical compression. Typically, shock reverberation[9–11], shock-ramp[12] and isentropic compression[13, 14] of planar samples by lasers or magnetic drive is used to reach a diverse array of states in a material sample of interest. However, due to the uniaxial compression, these techniques are limited in achievable density and pressure. To overcome these limitations, convergent geometries can be used. Shockless magnetically-driven cylindrical compression of beryllium liners to $\sim$ 5 Mbar has been demonstrated[15]. Magnetic compression of deuterium has been proposed in the past[16] and cylindrical compression of deuterium using explosives has been employed successfully to probe the deuterium Equation of State (EOS)[17]. Additionally, a spherical compression platform is currently under development at the National Ignition Facility[18]. The cylindrical compression method presented in this Letter allows a material sample to be compressed with a level of control not available using explosives while simultaneously maintaining a stagnated state for several nanoseconds for diagnosis. This opens the possibility of detailed measurements of both the stagnation dynamics and confinement properties of a highly converged fuel/liner system, as well as probing of the EOS of high pressure, high density matter.

An overview of our experiments is presented in Fig. 1. In these experiments, liquid deuterium filled cylindrical Be liners are compressed using the Z pulsed power accelerator at Sandia National Laboratories[19]. As the liner begins to move, a shock forms in the deuterium, which strengthens as it converges. The shock eventually strikes the axis of symmetry and reflects back towards the incoming liner, marking the onset of the deceleration phase of the implosion. The system stagnates when the sample and liner briefly come to pressure equilibrium before rapidly disassembling.

TABLE I: Parameters for deuterium compression experiments. For the liner, R_o is the outer liner radius and $AR \equiv R_o/\Delta R$ is the aspect ratio. The liner wall thickness is $\Delta R = 0.4$ mm for all targets. $\mathcal{CR}^{\rm meas}$ is the measured peak convergence ratio. For the deuterium, $\rho^{\rm sim}_{\rm stag}$ and $P^{\rm sim}_{\rm stag}$ are the simulated density and pressure at stagnation, respectively.

Z Shot #	R_o [mm]	AR	$\mathcal{CR}^{\rm meas}$	$\rho^{\rm sim}_{\rm stag}$ [g/cm^3]	$P^{\rm sim}_{\rm stag}$ [Gbar]
z2574	3.84	9.6	7.5	10	0.1
z2576	3.84	9.6	7.6	10	0.1
z2678	2.4	6	19	55	2

Using penetrating, 6.151-keV radiography[20–22], we have measured this stagnation process. The reflected shock is captured propagating outward, through the liner, after which the liner's inner surface reaches a minimum radius and begins to disassemble. This is the first time this sequence of events has been captured with radiography in such a way that the dynamics of the inner surface are still resolvable.

This platform is versatile, allowing for different current pulse shapes to control the strength of the initial shock launched into the sample. This control over the deuterium conditions in-flight allows us to tailor the stagnation state (i.e., thermally dominated or Fermi degenerate). Example magnetic pressure histories for the two different sets of experiments discussed here are shown in Fig. 1(c). The grey line is from the convergence ratio

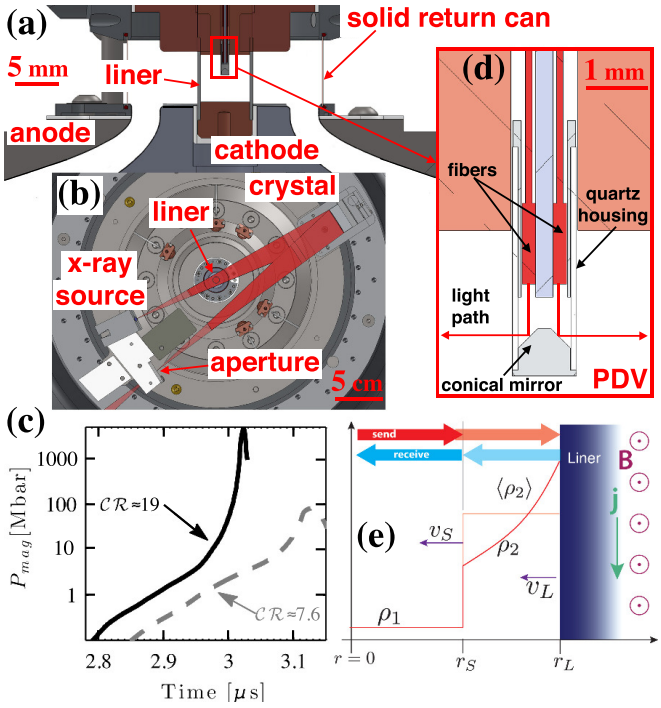

FIG. 1: (a) Drawing of the Be liner and the final electrical feed. (b) Top-down view of the experiment showing the backlighter geometry. The 6.151-keV x-rays generated at the source propagate through the liner and are collected by the crystal which focuses them through an aperture onto the detector (not shown). (c) Magnetic pressure histories for the 100 Mbar, $\mathcal{CR} = 7.6$ experiments (gray dashed) and the Gbar, $\mathcal{CR} = 19$ experiments (black solid). (d) Detail view of the radial PDV probe with two of the six fibers shown. The conical mirror directs the "send" laser light toward the liner and the "receive" light back into the fibers. (e) Schematic of the shock structure showing light reflected off of both the shock and liner, allowing v_S and v_L to be measured simultaneously.

7.6 ($\mathcal{CR} \equiv R^{\rm inner}_{\rm init}/R^{\rm inner}_{\rm final}$), 100 Mbar experiments. This pulse was designed to produce an isobaric stagnation profile at a relatively large radius ($\sim$ 500 μm). The black line shows the current pulse for the Gbar experiment, which was designed for a degeneracy pressure dominated stagnation at $\mathcal{CR} = 19$.

Figure 2 shows two of the four images taken from across shots $z2574$ and $z2576$ where identical targets and pulse shapes were used (see Table I for experimental parameters). Figures 2 (a) and (b) show the transmission radiographs converted to optical depth (OD), where OD is the natural log of the transmission. By Abel inverting the OD (assuming a constant opacity of 2.24 cm^2/g[23]), we obtain the density maps presented in Figs. 2 (c) and (d).

The liner's inner surface is clearly visible in these images. Figures 2(c) and (d) show a liner that is remarkably cylindrically symmetric and straight at the time of stagnation. Though the magneto Rayleigh-Taylor (MRT) instability[24] is present, and can be seen quite dramatically on the outer surface of the liner, feedthrough to the inner surface remains small. This experiment was designed and optimized by performing one- and two-dimensional simulations using the ALEGRA code[25]. The resulting density maps from the 2D simulation are shown in Fig. 2 (e) and (f). Comparing the simulated and measured density maps, we can see that the location and density of the liner's inner surface are in good agreement, though the evolution of the MRT instability on the outer surface is somewhat different.

The experimental density maps are used to determine the liner's inner radius as a function of time using each side of the image. The results are shown in Fig. 3 , where the squares indicate the mean and the error bars represent the standard deviation along the height. Also shown are the 1D simulated liner inner radius and velocity for comparison. The agreement between measurement and simulation is generally quite good, with the largest discrepancy appearing late in time, when the experimentally measured radius increases faster than predicted by simulation. This is not surprising, as the instabilities not captured in 1D grow and cause the liner to break apart reducing its ability to confine the deuterium.

The minimum radius is measured to be $R_{\rm i} = 452 \pm 21$ μm, giving a peak convergence ratio of $\mathcal{CR} = 7.6$. Because the targets are constructed with solid metal end caps, the deuterium cannot escape on the time scale of the implosion. Thus, we estimate the average deuterium density and areal density at minimum radius to be $\langle\rho\rangle = 10$ g/cm^3 and $\langle\rho r\rangle = 0.45$ g/cm^2. This was achieved with a peak current of 12 MA, requiring only 6 MJ of electrical energy stored in the Z accelerator's Marx capacitors.

The simulated liner velocity shows a sudden, impulsive deceleration just before the time of the first radiograph, due to the reflected shock from the axis striking the deuterium/liner interface. Indeed, looking at the abel inversion of the first radiograph (Figure 2 (c)) a discontinuous increase in density is observed within the liner wall. Taking lineouts of the density (Fig. 4 (a)) the discontinuity is seen traveling radially outward. A linear approximation to these points gives a shock velocity of $u_S \approx 30$ km/s (see Fig. 4(b)). The post-shock beryllium density is $\rho_2 \approx 16$ g/cm^3, while the unshocked beryllium has $\rho_1 \approx 8$ g/cm^3. The unshocked Be is moving radially inward at the implosion velocity ($v_1 \approx -25$ km/s from simulation). Using the Rankine-Hugoniot relations, we find the pressure change across the reflected shock

$$\Delta P = u_1^2 \rho_1 \left(1 - \frac{\rho_1}{\rho_2}\right) \approx 120 \text{ Mbar}, \qquad (1)$$

where $u_1 = u_s - v_1$ is the unshocked fluid velocity in the frame of reference moving with the shock.

In Fig. 4(b), the blue circles show the shock front position from the simulation. The simulated shock velocity is lower than measured, suggesting a lower shock pressure.

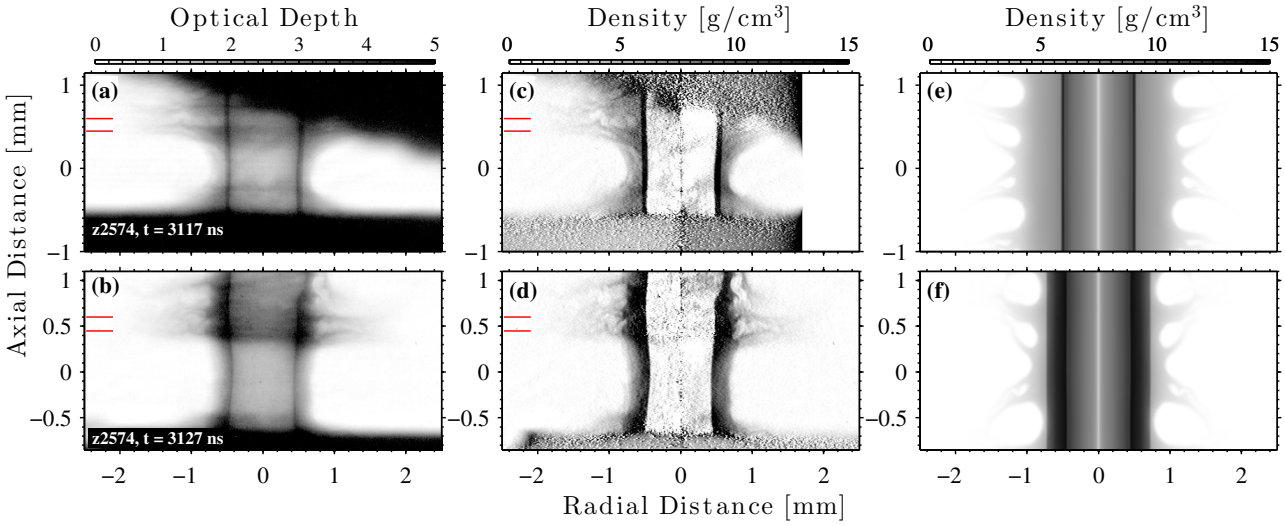

FIG. 2: (a)- (b) Transmission radiographs converted to optical depth with times indicated. Red lines indicate the region over which the image was averaged for shock analysis. (c)-(d) Be mass density profiles reconstructed using the Abel inversion technique. Images (a) and (c) are obstructed by an object partially blocking the beam path. (e)-(f) Mass profiles at the indicated times from 2D simulation.

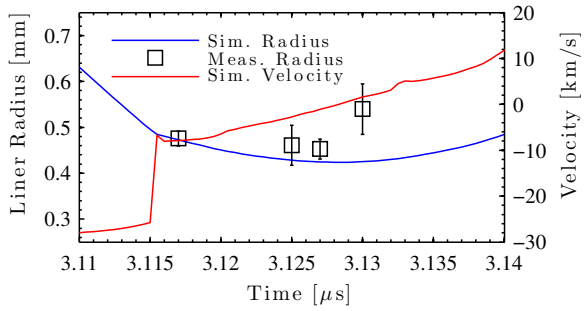

FIG. 3: Measured inner liner radius as a function of time compared to the simulated liner radius and velocity.

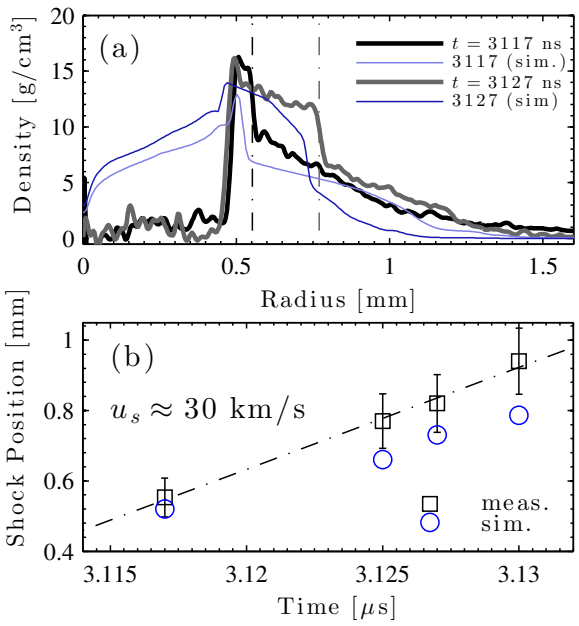

FIG. 4: (a) Be density lineouts (see red lines in Fig. 2(c)-(d)) showing the liner inner surface and the shock front. Blue lines show the simulated Be and deuterium density. (b) Measured shock position as a function of time with linear fit giving $u_S \approx 30$ km/s. Blue circles indicate the position of the shock front in the 1D simulation.

Indeed, the immediate simulated post-shock pressure in the Be is $80-90$ Mbar at the time of the first radiograph. As the shock reverberates in the deuterium, the pressure increases to 115 Mbar at the time of the last radiograph, in excellent agreement with the experimentally inferred pressure.

We have modified this platform to achieve higher density and pressure at stagnation by lowering the in-flight adiabat of the sample. This experiment was designed to achieve a degeneracy dominated stagnation with nearly uniform density profile at a pressure of $P_{stag} \approx 2$ Gbar and density of $\rho \approx 55$ g/cm^3. This is accomplished by modifying the magnetic pressure history (Fig. 1(c)) and liner radius (Table I) to achieve a lower in-flight adiabat.

We now consider the initial radially inward propagating shock in the deuterium during the early stages of the implosion. Photonic Doppler Velocimetry (PDV)[26] was used to measure the velocity of the liner's inner surface as well as the shock in the deuterium as a function of time during the implosion phase. Knowing both of these quantities allows us to determine the average post-shock state of the deuterium in flight, which is used to monitor

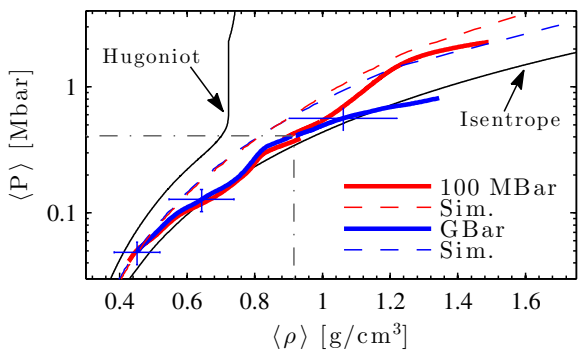

FIG. 5: Pressure vs. density plot showing the measured trajectory through phase-space for both the 100 Mbar (red) and Gbar (blue) experiments during implosion, ending when the deuterium shock strikes the PDV probe. Simulated average pressure and density are also shown for the 100 Mbar (dashed red) and Gbar (dashed blue) experiments. The principal Hugoniot and isentrope are shown for reference. Grey dashed lines indicate the deuterium state when the liner reflection is lost.

the change in sample adiabat. The probe, shown in Fig. 1(d), is similar to that used by Dolan *et al.*[27], except that the flat turning mirror is replaced with a conical one allowing measurements to be made at 6 equally spaced azimuths.

From Fig. 1(e) we see the unshocked state is characterized by density ρ_1 and the shocked medium is approximated by $\langle\rho_2\rangle$. The initial volume and density are known, and therefore, by integrating v_S and v_L to obtain the shock and liner positions, respectively, we can calculate $\langle\rho_2\rangle$. With this, the mean post-shock pressure can be estimated using the shock jump conditions.

The results of this analysis are shown for the two different experiments in Fig. 5. The solid lines show the experimentally unfolded average pressure vs. density trajectory for the 100 Mbar experiments in red and the Gbar experiment in blue. In both experiments, the reflection from the liner is lost at a density of ≈ 0.9 g/cm^3 and a pressure of ≈ 0.4 Mbar (indicated by the dashed gray lines). This loss of signal is likely due to an increased reflectivity of the shock front and/or an increase in absorptivity of the post-shock state. Above this, the simulated liner velocity is used in the analysis. Representative error bars are shown, derived by summing the contributions in quadrature due to uncertainty in the position of the shock when it first becomes reflective, the index of refraction of deuterium, and the extraction of the velocity histories from the raw PDV data. The thin dashed lines show the average post-shock density and pressure extracted from 1D simulations.

From this plot, it is seen that the deuterium adiabat is lower in the Gbar than the 100 Mbar experiment. In the Gbar experiment, the latest measurable state of the deuterium is $\langle\rho_2\rangle = 1.35$ g/cm^3 and $\langle \mathrm{P}_2\rangle = 0.8$ Mbar. At the same average density in the 100 Mbar experiment, the sample is at a pressure of $\langle \mathrm{P}_2\rangle = 1.9$ Mbar. Using the relation $P_i = \alpha_i \rho_i^{\gamma_i}$, where α_i is the sample adiabat in experiment i, we can estimate the reduction in adiabat as the ratio of the average pressures above, assuming the adiabatic index, γ, is the same in each case. This gives a reduction in adiabat of $\alpha_{\mathrm{Gbar}}/\alpha_{100\ \mathrm{Mbar}} \approx 0.4$.

Stagnation radiography was also employed on the Gbar experiment to confirm the predicted stagnation radius. We were unable to measure the reflected shock dynamics, but radiographs were obtained just before and near the time of minimum radius, the latter of which is shown in Fig. 6(a). While the backlighter provides a snapshot of the dynamics only during the time it is on, the detector is not time-gated. Therefore, emission from the target itself can contaminate the image. On this shot, due to the high pressure and convergence the target pinched, producing several bright spots that contaminated the images significantly (regions of negative OD). This makes quantitative analysis of the liner density difficult and prone to large errors. Pinching suggests late-time instability development; however we see good integrity of the liner's inner surface where it is visible, comparable to the lower pressure experiments. In Fig. 6(a), some curvature of the column is evident, indicating a very long wavelength asymmetry. Nevertheless, this does not appear to adversely affect the compression.

Despite the self-emission, the region of maximum optical depth (the *limb*), which corresponds to the liner's inner surface, is still visible through the regions of low liner ρR caused by the MRT instability. Lineouts were taken from the two cleanest portions of the image after a best-effort background correction was applied, shown in Fig. 6(b). The location of the limb is shown for each lineout (dashed lines). The smallest inner liner radius is $R_\mathrm{i} = 105$ μm, corresponding to $\mathcal{CR} = 19$, giving radially averaged $\langle\rho_D\rangle = 55$ g/cm^3 and $\langle\rho_D R\rangle = 0.5$ g/cm^2, in excellent agreement with the simulated stagnation conditions. By averaging the radius obtained in these two relatively clean regions, we obtain a mean stagnation radius of $\overline{R}_\mathrm{i} = 120$ μm, giving an average stagnation density of $\overline{\rho}_D = 47$ g/cm^3($\pm$25%).

Two-dimensional simulations were performed pre shot and again after the experiments were conducted using the measured load current and changing nothing else. The resulting pressure and density are shown in Fig.6(c). The simulated density map at stagnation was post-processed to obtain the optical depth as a function of radius; this is shown in Fig. 6(b) as the thin red line (scaled arbitrarily for clarity). The location of the limb is in very good agreement with the blue line, indicating excellent agreement with the measured deuterium compression. However, the simulated profile is substantially wider. By measuring the width from $10-90\%$, we find that the experimental width is ≈ 60 μm while the simulated width

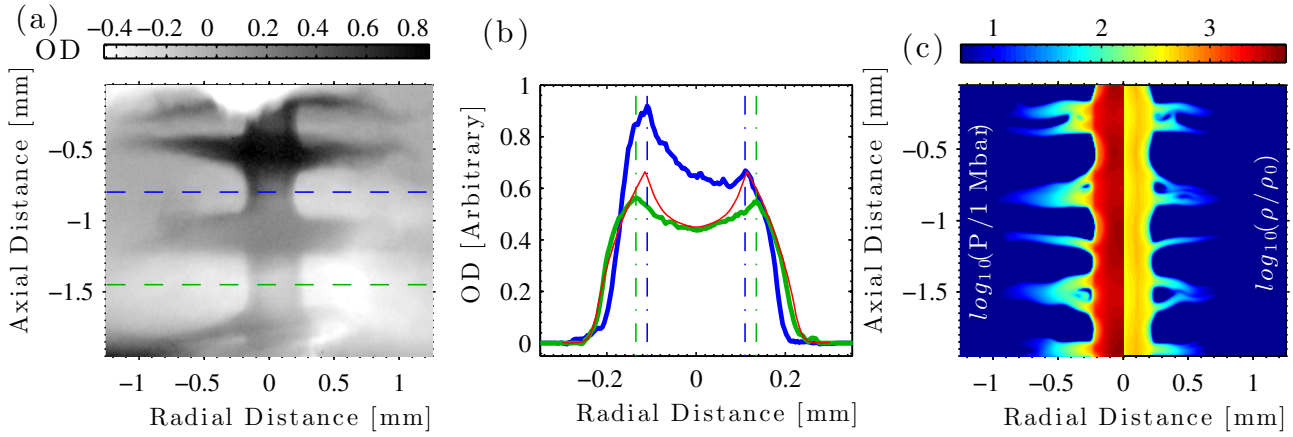

FIG. 6: (a) Radiograph, converted to OD, of a Be liner stagnating at $P_{\rm stag} \sim 2$ Gbar. (b) Lineouts of the OD with colors corresponding to the locations of the respective horizontal lines in (a). Units of OD are arbitrary due to the unknown level of self-emission. Vertical lines denote the location of peak OD corresponding to the location of the inner liner surface. The simulated OD is included (thin red line), scaled for clarity. (c) Results of the 2D simulation taken at the time corresponding to the radiograph in (a). Left side corresponds to the log of pressure in Mbar. Right side corresponds to the log of density divided by the initial density of liquid deuterium (0.17 g/cm^3).

is ≈ 100 μm. This may be in part due to the background correction, but is most likely due to discrepancies in the simulated evolution of the MRT instability and the resulting redistribution of mass.

By examining the simulated pressure and density we can estimate the experimental conditions achieved. The deuterium density ranges from 30 g/cm^3 on axis to 65 g/cm^3 at the liner/deuterium interface. The pressure is very uniform across the sample at 2.25 Gbar. The temperature peaks on axis at ≈ 80 eV and decays to just a few eV at the liner wall, corresponding to a mass average of $T = 10$ eV. This gives a mass averaged plasma parameter $\Gamma = ze^2/ak_BT \approx 6$, indicating the deuterium is strongly coupled at stagnation.

It has long been known that magnetic compression can produce extreme pressure if current can reliably be brought to small radius. These experiments show that it is possible, and quite practical, to do this. We have demonstrated a platform that allows the study of dynamics of stagnating systems at conditions relevant to ICF, and at spatial scales that are straightforward to diagnose. Additionally, with improved diagnostic techniques, this platform can allow off-hugoniot studies of the EOS of deuterium as well as other materials. Advanced diagnostics, such as x-ray Thomson scattering, can be employed to characterize the in-flight post-shock state as well as the stagnation state of the material sample, providing unprecedented access to these extreme conditions. Furthermore, samples like this can, in principle, be used to study other properties of compressed matter, such as charged particle stopping powers, x-ray opacities, and atomic kinetics.

The authors would like to thank Dr. Brent Blue and Kurt Tomlinson of General Atomics for their work in designing and fabricating the radial PDV probe. Sandia National Laboratories is a multi-program laboratory managed and operated by Sandia Corporation, a wholly owned subsidiary of Lockheed Martin Corporation, for the U.S. Department of Energy's National Nuclear Security Administration under contract DE-AC04-94AL85000.

[1] D. Saumon and T. Guillot, The Astrophysical Journal **609**, 1170 (2004).
[2] T. Guillot, Science **286**, 72 (1999), http://www.sciencemag.org/content/286/5437/72.full.pdf, URL `http://www.sciencemag.org/content/286/5437/72.abstract`.
[3] G. Chabrier, D. Saumon, and A. Y. Potekhin, Journal of Physics A: Mathematical and General **39**, 4411 (2006).
[4] A. Becker, W. Lorenzen, J. J. Fortney, N. Nettelmann, M. Sch?ttler, and R. Redmer, The Astrophysical Journal Supplement Series **215**, 21 (2014).
[5] R. Redmer, B. Holst, H. Juranek, N. Nettelmann, and V. Schwarz, Journal of Physics A: Mathematical and General **39**, 4479 (2006).
[6] J. Nuckolls, L. Wood, A. Thiessen, and G. Zimmerman, Nature **239**, 139 (1972).
[7] J. Lindl, Phys. Plasmas **2**, 3933 (1995).
[8] O. A. Hurricane, D. A. Callahan, D. T. Casey, P. M. Celliers, C. Cerjan, E. L. Dewald, T. R. Dittrich, T. Doppner, D. E. Hinkel, L. F. B. Hopkins, et al., Nature **506**, 343 (2014).
[9] R. W. Lemke, M. D. Knudson, D. E. Bliss, K. Cochrane, J.-P. Davis, A. A. Giunta, H. C. Harjes, and S. A. Slutz, Journal of Applied Physics **98**, 073530 (2005).
[10] M. D. Knudson, D. L. Hanson, J. E. Bailey, C. A. Hall,

J. R. Asay, and C. Deeney, Phys. Rev. B **69**, 144209 (2004).
[11] D. C. Swift, T. E. Tierney, R. A. Kopp, and J. T. Gammel, Phys. Rev. E **69**, 036406 (2004).
[12] D. C. Swift, R. G. Kraus, E. N. Loomis, D. G. Hicks, J. M. McNaney, and R. P. Johnson, Phys. Rev. E **78**, 066115 (2008).
[13] C. A. Hall, J. R. Asay, M. D. Knudson, W. A. Stygar, R. B. Spielman, T. D. Pointon, D. B. Reisman, A. Toor, and R. C. Cauble, Review of Scientific Instruments **72** (2001).
[14] J.-P. Davis, C. Deeney, M. D. Knudson, R. W. Lemke, T. D. Pointon, and D. E. Bliss, Phys. Plasmas **12**, 056310 (2005).
[15] M. R. Martin, R. W. Lemke, R. D. McBride, J.-P. Davis, D. H. Dolan, M. D. Knudson, K. R. Cochrane, D. B. Sinars, I. C. Smith, M. Savage, et al., Phys. Plasmas (2012).
[16] M. Weinwurm, S. N. Bland, and J. P. Chittenden, Physics of Plasmas (1994-present) **20**, 092701 (2013), URL `http://scitation.aip.org/content/aip/journal/pop/20/9/10.1063/1.4820805`.
[17] V. E. Fortov, R. I. Ilkaev, V. A. Arinin, V. V. Burtzev, V. A. Golubev, I. L. Iosilevskiy, V. V. Khrustalev, A. L. Mikhailov, M. A. Mochalov, V. Y. Ternovoi, et al., Phys. Rev. Lett. **99**, 185001 (2007).
[18] A. Kritcher, T. Dppner, D. Swift, J. Hawreliak, G. Collins, J. Nilsen, B. Bachmann, E. Dewald, D. Strozzi, S. Felker, et al., High Energy Density Physics **10**, 27 (2014), ISSN 1574-1818.
[19] M. Savage, K. LeChien, W. Stygar, J. Maenchen, D. McDaniel, and K. Struve, in *IEEE International Power Modulators and High Voltage Conference, Proceedings of the 2008* (2008), pp. 93–93.
[20] G. R. Bennett, I. C. Smith, J. E. Shores, D. B. Sinars, G. Robertson, B. W. Atherton, M. C. Jones, and J. L. Porter, Rev. Sci. Instrum. **79**, 10E914 (2008), ISSN 00346748.
[21] R. D. McBride, S. A. Slutz, C. A. Jennings, D. B. Sinars, M. E. Cuneo, M. C. Herrmann, R. W. Lemke, M. R. Martin, R. A. Vesey, K. J. Peterson, et al., Phys. Rev. Lett. **109**, 135004 (2012).
[22] R. D. McBride, M. R. Martin, R. W. Lemke, J. B. Greenly, C. A. Jennings, D. C. Rovang, D. B. Sinars, M. E. Cuneo, M. C. Herrmann, S. A. Slutz, et al., Phys. Plasmas **20**, 056309 (pages 10) (2013).
[23] The opacity assumed here applies to the beryllium only. The deuterium has a much lower opacity and, therefore, does not significantly absorb the backlighter radiation. For this reason, the abel inverted density maps appear hollow for the experiment, despite the high density of deuterium at stagnation. In contrast, the simulated maps show the total mass density and therefore the deuterium is apparent.
[24] E. G. Harris, Phys. Fluids **5**, 1057 (1962), ISSN 00319171.
[25] A. C. Robinson, T. A. Brunner, S. Carroll, R. Drake, C. J. Garasi, T. Gardiner, T. Haill, H. Hanshaw, D. Hensinger, D. Labreche, et al., in *Proceedings of the 46th AIAA Aerospace Sciences Meeting and Exhibit, 7–10 January 2008, Reno, Nevada* (AIAA, 2008).
[26] O. T. Strand, D. R. Goosman, C. Martinez, T. L. Whitworth, and W. W. Kuhlow, Review of Scientific Instruments **77**, 083108 (2006).
[27] D. H. Dolan, R. W. Lemke, R. D. McBride, M. R. Martin, E. Harding, D. G. Dalton, B. E. Blue, and S. S. Walker, Rev. Sci. Instrum. **84**, 055102 (2013).